ISSN 1063-7842, Technical Physics, 2015, Vol. 60, No. 9, pp. 1343–1347. © Pleiades Publishing, Ltd., 2015.
Original Russian Text © S.K. Lazarouk, P.S. Katsuba, A.A. Leshok, V.B. Vysotskii, 2015, published in Zhurnal Tekhnicheskoi Fiziki, 2015, Vol. 85, No. 9, pp. 86–90.

PHYSICAL SCIENCE OF MATERIALS

Effect of the Local Electric Field on the Formation of an Ordered Structure in Porous Anodic Alumina

S. K. Lazarouk*, P. S. Katsuba, A. A. Leshok, and V. B. Vysotskii

Belarussian State University of Informatics and Radioelectronics, Minsk, 220013 Belarus
**e-mail: serg@nano.bsuir.edu.by*

Received November 28, 2014

Abstract—Experimental data and a model are presented, and the electric field that appears in porous alumina during electrochemical anodic oxidation of aluminum in electrolytes based on an aqueous solution of oxalic acid at a voltage of 90–250 V is calculated. It is found that the electric field in the layers with a porosity of 1–10% in growing alumina reaches 10^9–10^{10} V/m, which exceeds the electric strength of the material and causes microplasma patterns emitting visible light at the pore bottom, the self-organization of the structure of porous alumina, and the anisotropy of local porous anodizing. Moreover, other new effects are to be expected during aluminum anodizing under the conditions that ensure a high electric field inside the barrier layer of porous oxide.

DOI: 10.1134/S1063784215090108

INTRODUCTION

Porous alumina is used in microelectronics as an interlevel insulator in the systems of multilayer interconnection elements in integrated circuits [1]. The use of an ordered cellular structure of this material in nanoelectronic circuits is also of particular interest [2–5]. The structure of porous alumina undergoes self-organization when it forms during electrochemical anodic oxidation of aluminum at high forming voltages [6, 7]. In this case, the electric field increases locally inside the barrier layer of porous alumina at the boundary with an electrolyte during anodizing, which influences the anodic process kinetics and the order of a formed porous structure. The purpose of this work is to study the structure of porous anodic alumina, to refine a structural model, to calculate the electric field distribution inside the barrier layer of porous alumina, and to propose a mechanism to explain the self-organization of hexagonal alumina cells at a high voltage during the anodic process.

EXPERIMENTAL

Porous alumina films were formed in electrolytes based on an aqueous solution of oxalic acid with a concentration of 0.05–1 M at an electrolyte temperature of 24 ± 2°C. Anodizing was carried out at a high voltage, from 90 to 250 V, and the anode current density was 50–200 mA/cm^2. To perform an anodic process at a high voltage and anode current, we used anodizing in the meniscus region or local anodizing with a photolithographic mask [8, 9]. The geometric sizes of alumina cells were determined by scanning electron microscopy.

POROUS LAYER MODEL

The porous layer was represented in the form of close-packed hexagonal alumina cells each of which consists of a hexagonal prism with a cylindrical pore at the center and a barrier layer at the boundary with a metallic surface (Fig. 1) [10]. The barrier layer is the space between the lower base of the hexagonal prism and a spherical segment. A single cell is described by the following structural parameters: R_0 is the radius of the spherical segment of the pore bottom, R_S is the radius of the spherical segment of the hexagonal cell at the oxide–metal interface, α_0 is half the angle of the spherical cone of the pore bottom, α_S is half the angle of the spherical cone of the oxide–metal interface, L is the center distance between pores, and d is the pore diameter.

Let us consider these parameters in more detail. For example, the angle of the spherical cone at the oxide–metal interface is $2\alpha_S$. To calculate it, we consider a right-angled triangle with side $L/2$ and hypotenuse R_S. Then, we have

$$\sin\alpha_S = \frac{L}{2R_S} \quad (1)$$

and, correspondingly,

$$\alpha_S = \arcsin\frac{L}{2R_S}. \quad (2)$$

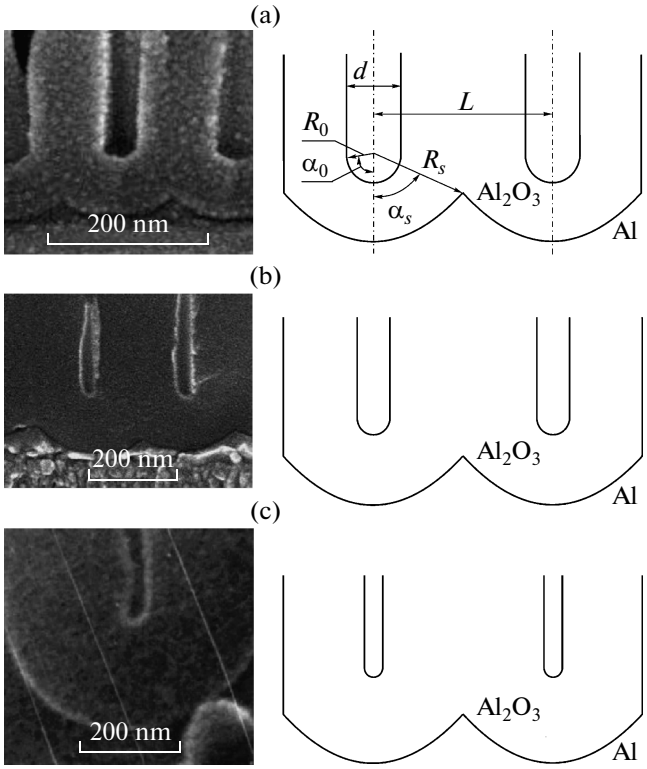

Fig. 1. Micrographs and the corresponding schematic images of the cross section of the porous alumina cells formed in oxalic acid electrolytes of various concentrations ((a) 1 M $H_2C_2O_4$, (b) 0.2 M $H_2C_2O_4$, (c) 0.05 M $H_2C_2O_4$) at a voltage of 90, 160, and 250 V, respectively.

By analogy, we obtain

$$\alpha_0 = \arcsin\frac{d}{2R_0}. \quad (3)$$

The area of the segment of a sphere S_{segm} is calculated as

$$S_{segm} = 2\pi R_{segm} h_{segm}, \quad (4)$$

where h_{segm} is the height of the segment of a sphere and R_{segm} is the radius of the segment of a sphere.

Here, the difference between the area of the segment of a sphere and the real boundary area of the barrier layer of a single cell (the projection of which on a horizontal plane is a hexahedron) is neglected.

The height of the segment of a sphere h_{segm} is calculated through its radius R_{segm} and angle α_{segm},

$$h_{segm} = R_{segm}(1 - \cos\alpha_{segm}). \quad (5)$$

Then, the area of the segment of a sphere is

$$S_{segm} = 2\pi R_{segm}^2(1 - \cos\alpha_{segm}). \quad (6)$$

Correspondingly, the area of the segment of a sphere of the pore bottom is

$$S_0 = 2\pi(R_S - R_0)^2(1 - \cos\alpha_0). \quad (7)$$

The minimum electric field in the barrier layer of the porous alumina cells is estimated using the formula for a homogeneous field,

$$E_{min} = \frac{U_a}{\varepsilon(R_S - R_0)}, \quad (8)$$

where ε is the permittivity of anodic alumina (equal to 8) [10].

Since all lines of forces of the electric field meet at the pore bottom, the electric field distribution in the barrier layer can be expressed as

$$E(r) = \frac{E_{min} 2\pi R_{segm}^2(1 - \cos\alpha_S)}{S_{pore}}, \quad (9)$$

where $R_{segm} = R_S - r$ takes the values from R_0 to R_S.

When making a substitution, we derive the following final formula to calculate the electric field distribution inside the barrier layer:

$$E(r) = \frac{U_a(R_S - r)^2(1 - \cos\alpha_S)}{\varepsilon R_0^2(R_S - R_0)(1 - \cos\alpha_0)}, \quad (10)$$

where r changes from 0 to $R_S - R_0$.

To illustrate the calculation results, we introduce new dimensionless quantity Δx, which characterizes the position of a point inside the barrier layer beginning from the pore bottom ($\Delta x = 0$) to the boundary between the barrier layer and aluminum ($\Delta x = 1$) (i.e., Δx is the ratio of the distance between the point and the pore bottom to the barrier layer thickness),

$$\Delta x = \frac{r}{R_s - R_0}, \quad r = \Delta x(R_S - R_0).$$

Then, the final formula takes the form

$$E(r) = \frac{U_a(R_S - \Delta x(R_S - R_0))^2(1 - \cos\alpha_S)}{\varepsilon R_0^2(R_S - R_0)(1 - \cos\alpha_0)}, \quad (11)$$

where Δx changes from 0 to 1.

The numerical calculations of the spatial distribution of the electric field in experimental structures were carried out using the COMSOL Multiphysics software package by solving Poisson's equation for a given configuration of conducting and dielectric regions and by solving the geometric problem of calculating the ratio of the areas of the spheres in the barrier layer with various radii of these segments.

RESULTS AND DISCUSSION

Figure 1 shows micrographs of the cross section of porous alumina cells formed in oxalic acid electrolytes of various concentrations. They show that the porosity decreases with decreasing oxalic acid concentration in an electrolyte, which indicates an increase in the local electric field strength inside anodic alumina.

Figures 1a–1c also schematically depict porous alumina cells for a porosity of 10, 3, and 1%. The table gives the conditions of formation and the structural parameters of the porous oxide films, which were used to calculate the electric field distribution inside the barrier layer of porous alumina with various configurations of hexagonal cells. Note that the porosity range obtained for each electrolyte covers 1, 3, and 10%, respectively.

Figure 2 shows the results of calculating the electric field distribution for three barrier layer configurations, the parameters of which are presented in the table (average values were used for the calculation). The abscissa is the relative position of a point inside the barrier layer: zero corresponds to the electrolyte–barrier layer interface, and unity corresponds to the metal–barrier layer interface.

The calculation results demonstrate that the electric field in the barrier layer at the interface with an electrolyte is more than an order of magnitude higher than the electric field at the barrier layer–aluminum interface (Fig. 2). Thus, the barrier layer–electrolyte interface at the pore bottom is the "hottest" place.

Figure 3 depicts the results of calculating the electric field inside porous alumina with a porosity of 1.2%. The discrepancy between the results of calculations performed by different methods does not exceed 10%, which indicates a sufficiently high reliability of the calculation results. Moreover, it should be noted that the porous alumina films with a porosity of 1.2% were formed at an electric field of about 10^{10} V/m. Such a high value cannot be obtained in bulk materials: this effect is only observed in nanostructures. In this case, the electric field approaches the intraatomic electric field (~10^{11} V/m) [10]. Fundamentally new effects, as in the case of nonlinear optics, appear

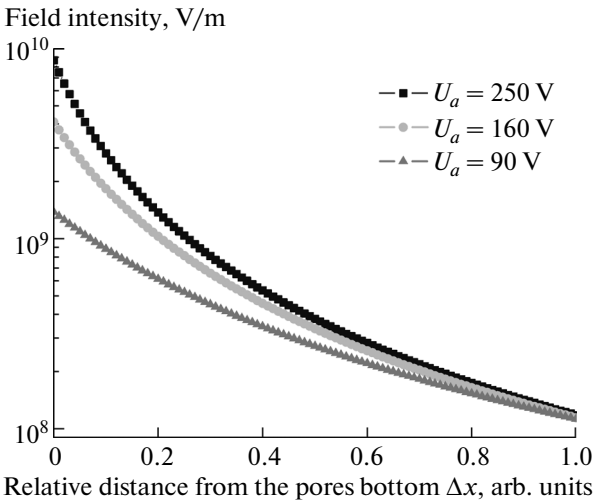

Fig. 2. Electric field distribution in the barrier layer from the pore bottom (zero in abscissa) to the oxide–metal interface (unity in abscissa) for the structures the parameters of which are given in the table.

Forming conditions and the structural parameters of porous alumina

Electrolyte	U_a, V	R_s, nm	R_0, nm	L, nm	d, nm	P, %
0.05 M	250	280–320	30–40	480–520	50–70	1–2
0.2 M	160	190–230	30–40	330–370	50–65	2–3
1 M	90	130–150	35–45	210–250	65–75	8–10

in such nanostructures [11]. In particular, we observed microplasma patterns in the form of bright points in the field of an optical microscope during the anodic process (Fig. 4). The lifetime of such microplasma patterns is several fractions of a second, and their density increases with the voltage.

Note that microplasma patterns are only observed when oxides with a porosity less than 1% form, when the electric field at the pore bottom is higher than 10^{10} V/m. The appearance of such microplasma patterns is thought to be preceded by the formation of plasma nanoregions at sites with a high electric field. These sites are located in the barrier layer of anodic oxide near the pore bottom. These plasma nanoregions are thought to favor the self-organization of porous anodizing due to their localization strictly at the center of the formed hexagonal cells. This assumption is supported by the fact that the organization of porous alumina is most pronounced at high voltages before the formation of microplasma patterns, which are localized in significantly larger regions and, thus, break nanosized self-organization (Fig. 5). Plasma nanoregions are invisible, since their sizes are smaller than the resolution of the optical microscope. Such plasma nanoregions can play the role of self-focusing seeds for pore growth, which ensures self-organization of the structure of the growing porous oxide. Note that this phenomenon is analogous to the effect of self-focusing of a light beam in nonlinear optics in an electric field of 10^{10}–10^{11} V/m.

Another new effect, which appears during porous anodizing of aluminum at a high voltage, is the anisotropy of anode growth with a masking coating. This

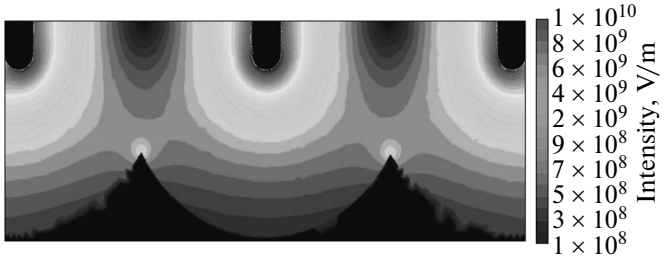

Fig. 3. Schematic two-dimensional electric field distribution inside the barrier layer for the cross section of porous alumina cells with configuration 1 from the table (logarithmic scale, V/m).

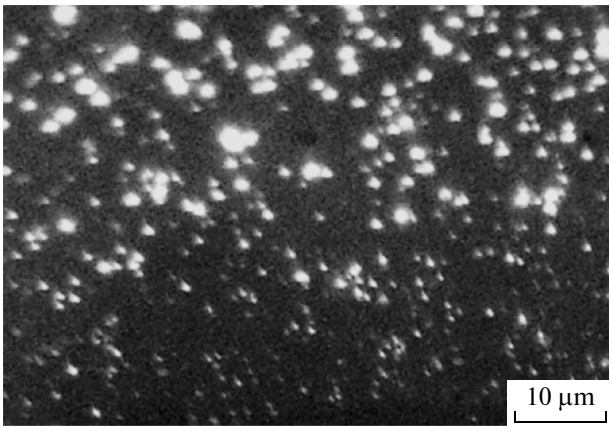

Fig. 4. Microplasma patterns observed with an optical microscope during porous anodizing of aluminum in 0.05 M $H_2C_2O_4$ at a voltage of 270 V.

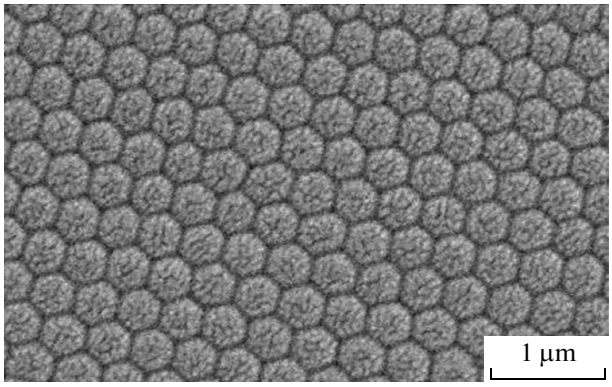

Fig. 5. Photograph of the frontal surface of porous alumina formed in 0.05 M $H_2C_2O_4$ at a voltage of 200 V.

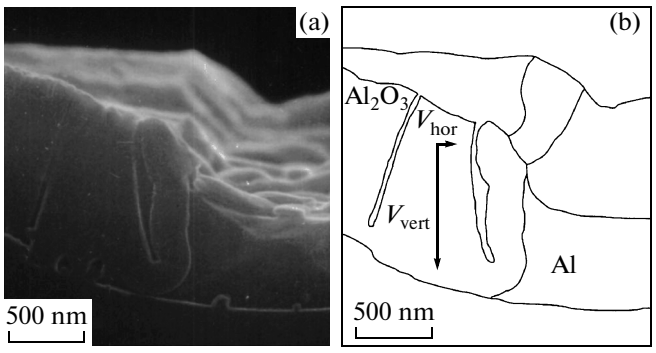

Fig. 6. (a) Photograph of the cross section of porous alumina formed by local anodizing in 0.05 M $H_2C_2O_4$ at a voltage of 250 V and (b) schematic image of porous alumina demonstrating predominant pore growth in the vertical direction with respect to the initial surface.

anisotropy consists in a noticeable difference between the anodic oxide growth rate in the vertical (V_{vert}) and horizontal (V_{hor}) directions, which ensures the minimum lateral drifts during the formation of the pattern specified by a mask (mask in Fig. 6 is removed). Note that porous anodizing at low voltages is isotropic: the process rate in the horizontal and vertical directions is almost the same [12].

The formation of aluminum interconnections in integrated circuits using porous anodizing of aluminum at a high degree of anisotropy makes it possible to use this process to produce VLSI metallization with a submicron element size [13] and opens up fresh opportunities for the integration of optical and metallic interconnections on silicon chips [14].

Thus, our studies showed that the electric field in local regions inside oxide during porous anodizing of aluminum at a high voltage reaches 10^9–10^{10} V/m, which can cause fundamentally new effects. These effects can include the self-organization of a porous structure, the appearance of microplasma patterns, and an anisotropy of porous anodizing. Moreover, other new effects are to be expected during aluminum anodizing under conditions that ensure a high electric field inside the barrier layer of porous oxide.

CONCLUSIONS

The calculation of the electric field created in alumina during aluminum anodizing showed that it is high in the barrier layer near the electrolyte–oxide interface for structures with low porosity. The experimental results demonstrate that such high fields cause microplasma patterns emitting visible light at the pore bottom, the self-organization of the structure of porous alumina, and the anisotropy of local porous anodizing.

ACKNOWLEDGMENTS

We thank Prof. V.E. Borisenko for useful discussions.

This work was performed in terms of the state program "Functional Materials, Composites, and Nanomaterials" of Republic of Belarus (project no. 2.4.18).

REFERENCES

1. S. Lazarouk, S. Katsouba, A. Leshok, A. Demianovich, V. Stanovski, S. Voitech, V. Vysotski, and V. Ponomar, Microelectron. Eng. **50**, 321 (2000).
2. P. Katsuba, P. Jaguiro, S. Lazarouk, and A. Smirnov, Physica E **41**, 931 (2009).
3. S. K. Lazarouk, A. A. Leshok, V. A. Labunov, and V. E. Borisenko, Semiconductors **36**, 149 (2005).
4. G. D. Sulka and K. Hnida, Nanotechnology **23**, 075303 (2012).
5. O. M. Golitsyna, S. N. Drozhdin, I. E. Zanin, and A. E. Gridnev, Phys. Solid State **54**, 2296 (2012).
6. S. Chu, K. Wada, S. Inoue, M. Isogai, and A. Yasumori, Adv. Mater. **17**, 2115 (2005).

7. C. Cheng and A. H. W. Ngan, Nanotechnology **24**, 215602 (2013).
8. S. K. Lazarouk, D. A. Sasinovich, V. E. Borisenko, A. Muravski, V. Chigrinov, and H. S. Kwok, J. Appl. Phys. **107**, 033527 (2010).
9. S. K. Lazarouk, *Physics, Chemistry and Application of Nanostructures* (World Sci., Singapore, 2013), pp. 355–358.
10. L. Young, *Anodic Oxide Films* (Academic, New York, 1961).
11. *Encyclopedia of Physics*, Ed. by A. M. Prokhorov (Bol'shaya Ross. Entsiklopediya, Moscow, 1992).
12. S. Lazarouk, I. Baranov, G. Maello, E. Proverbio, G. De Cesare, and A. Ferrari, J. Electrochem. Soc. **141**, 2556 (1994).
13. S. Lazarouk, S. Katsouba, A. Demianovich, V. Stanovski, S. Voitech, V. Vysotski, and V. Ponomar, Solid State Electron. **44**, 815 (2000).
14. S. K. Lazarouk, A. A. Leshok, P. S. Katsuba, and V. E. Borisenko, in *Proceedings of the 24th International Crimean Conference on Microwave and Telecommunication Technology, Sevastopol', 2014*, pp. 800–802.

Translated by K. Shakhlevich